ChemComm

Accepted Manuscript

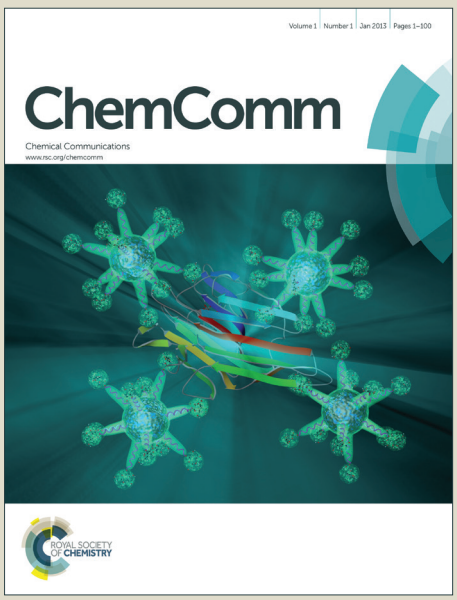

ROYAL SOCIETY OF CHEMISTRY

www.rsc.org/chemcomm

Cite this: DOI: 10.1039/c0xx00000x

www.rsc.org/xxxxxx

COMMUNICATIONS

Pt-free solar driven photoelectrochemical hydrogen fuel generation using 1T MoS_2 co-catalyst assembled CdS QDs/TiO_2 photoelectrode

R. Raja,[a] P. Sudhagar,[b*] Anitha Devadoss,[b] C. Terashima,[b] L. K. Shrestha,[c] K. Nakata,[b] R. Jayavel,[a*] K. Ariga,[c] and A. Fujishima[b]

Received (in XXX, XXX) Xth XXXXXXXXX 20XX, Accepted Xth XXXXXXXXX 20XX
DOI: 10.1039/b000000x

The solar to hydrogen generation from TiO_2-CdS-ZnS-MoS_2 (*TCZM*) heterointerface was demonstrated. We found that Pt free CdS quantum dot sensitized TiO_2 mesoporous electrode with metallic-type 1T MoS_2 co-catalyst resulted 0.11 ml/cm^{-2}h^{-1} H_2 fuel generation under unassisted potential mode, which was strikingly promoted to 1.47 ml/cm^{-2}h^{-1} upon 1 V applied potential.

The energy generation from fossil fuel sources having foremost issues on existing undesirable CO_2 emission in atmosphere and depletion of their resource from earth also predicts a huge demand in energy consumption. Therefore, generating inexpensive, pollution-free fuels (hydrogen and oxygen) is a challenging task to the mankind. Hydrogen (H_2) is the easiest multisource component in view of gaseous fuel or electron-rich precursor to liquid transportation fuel. Though the hydrogen fuel generation from water using solar energy through 'artificial photosynthesis' process was demonstrated four decades ago,[1] the recent energy demand fosters 'solar fuel conversion' as an emerging technology. The photo electrochemical (PEC) cells are also considered as powerful tool in transforming solar light into hydrogen fuel with appropriate electrolyte and semiconductor electrodes.[2] However, the challenging task in PEC process is designing the visible light semiconductors for tracking major fraction of solar energy with effective charge separation (e^- and h^+) at electrode/electrolyte interfaces.[3]

Recently, the combinatorial approach of assembling low-dimensional semiconducting 'quantum-dot' (QDs: CdS, CdSe, PbS, etc) with wide band gap metal oxides (TiO_2, ZnO, and WO_3) showed striking PEC H_2 generation performance owing to the unique properties of QDs (high absorbance co-efficient, multiple carrier generation and fast charge separation).[4] In this line, new type of electrode-architectures like 'quasi artificial leaf', 'panchromatic (QD/dye) sensitizer' and 'high light reflector' explored with Pt counter electrodes realize the QDs as futuristic candidate in PEC H_2 generation.[5] Conversely, in view of fabricating low-cost, Pt-free photocatalytic assemblies for hydrogen generation, a broad range of metal sulphides (CdS, CdSe, $Cd_{1-x}Zn_xS$, $Zn_{1-x}Cd_xS$, $Zn_{1-x}In_xS$)[6] were explored in the form of solid solution, nevertheless only very few works were reported on electrode architecture.[7] Despite the above mentioned Pt-free metal sulphide photocatalyst systems showed feasible quantum yield, still their performance is inferior to the Pt catalyst systems. One of the prospective approaches is enhancing the catalytic active sites by implementing atomic scale layered co-catalyst on the photocatalyst assemblies. In this context, thin atomic layer of MoS_2 received great attention in graphene analogue layered transition metal dichalcogenide.[8] The striking features of edge controlled MoS_2 catalytic properties render effective performance in electrocatalytic and photocatalytic hydrogen evolution reaction.[8c, 9] The previous studies on CdS/MoS_2 in the form of suspended photocatalyst endorse new pathways in MoS_2 based solar fuel generation.[10] However limited internal surface area for dual functionality of water oxidation (with sacrificial donor) and reduction process on same CdS/MoS_2 solid interfaces limits the solar fuel yield and necessitates the execution as separate counterpart in the form of electrode.

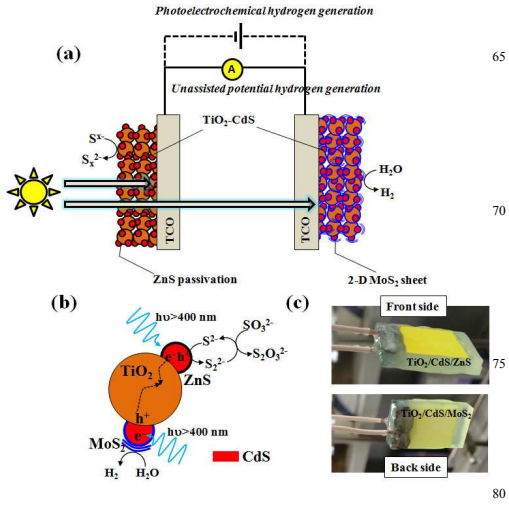

Scheme 1. (a) Schematic illustration of double-sided photoelectrode with TiO_2-CdS-ZnS (anode) and TiO_2-CdS-MoS_2 electrodes (cathode); (b) proposed mechanism of PEC hydrogen generation at TiO_2-CdS-ZnS-MoS_2 heterointerfaces through Z-scheme process under light irradiation (>400 nm); (c) photography of back-to-back assembled electrodes.

In the present work, we demonstrate the *TCZM* heterointerfaces in tandem electrode configuration and accomplish their solar to hydrogen fuel generation as is illustrated in Scheme 1a. The *CdS/ZnS* and *CdS/MoS_2* were assembled on mesoporous TiO_2 electrode and configured as photoanode and counter electrode, respectively. It can be envisioned that this approach may be

employed to controlling the properties of each layer independently compared with one-pot synthesized powder type sample. To the best of our knowledge, this is the first report that showcases the application of *TCZM* heterointerfaces in tandem electrode configuration for solar hydrogen fuel generation. For further experimental details of preparing TiO_2 mesoporous electrodes, CdS QDs sensitization and coating of chemically exfoliated MoS_2 sheets on TiO_2/CdS QDs refer **supporting information S1** and SEM images in **Fig.S2**. Under visible light irradiation (>400 nm), the excitons (e^-/h^+) were generated at CdS and electrons were transport to the charge collector through TiO_2 layer. Conversely, holes were scavenged by electrolyte species and produce H^+ carriers in the electrolyte. Concurrently, the fraction of the light illumination transmitted through photoanode will reach TiO_2/CdS/MoS_2 counter electrode (CE) and perform analogous function with photoanode. Under unassisted bias condition, the photoelectrons collected from anode will be directed to CE side, where they will recombine with the photoholes at TiO_2 surface through Z-scheme mechanism (Scheme 1b). The remaining photoelectrons generated at CdS (CE side) will be injected to MoS_2 co-catalyst and perform H^+ ions reduction into hydrogen fuel. The schematic photocatalytic mechanism is illustrated in Scheme 1b

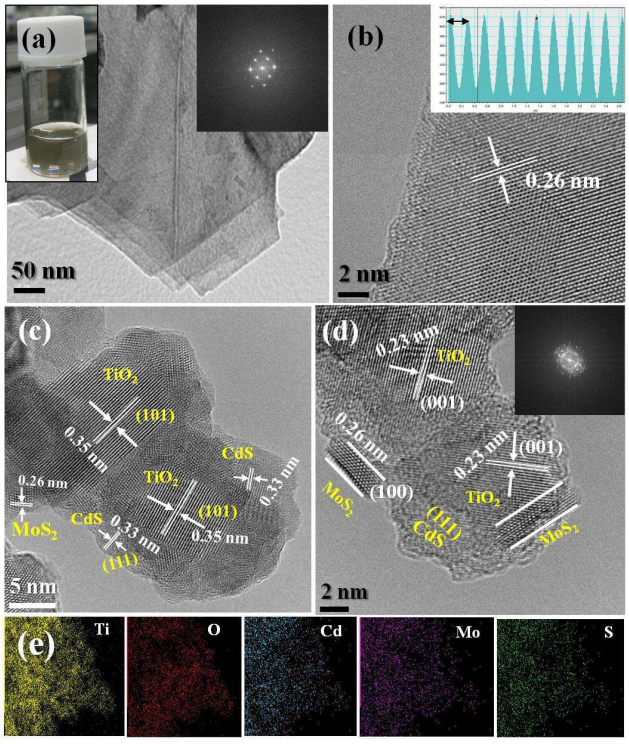

Figure 1. TEM images of exfoliated MoS_2 sheets (inset: photography of MoS_2 exfoliated solution and SAED pattern); (b) HRTEM image of MoS_2 nanosheet (inset: distance between lattice fringes at 1T MoS_2 phase); (c) and (d) HRTEM images of TiO_2-CdS-MoS_2 at different locations (inset: SAED pattern); (e) EDS mapping of Ti,O,Cd, Mo and S.

The TEM image of chemically exfoliated MoS_2 is presented in Fig. 1(a), and it seems to have two dimensional (2-D) few layer stacked sheet-like morphology with lateral dimension of ~500-700 nm. At high magnification (2nm) scale (Fig.1b), a single layer of 2-D MoS_2 exhibit biphase crystallite structure with clear grain boundary (**See supporting information S3**). In accord to Eda *et al*.,[11] the honeycomb lattice structure (Fig.S3) indicates the trigonal prismatic (2H) and hexagonal lattice corresponding to the octahedral geometry (1T). This clearly demonstrates that exfoliated 2-D sheets can produce atomically thin layers of (002) crystallite facet of MoS_2. The lattice space values of 2H and 1T layers were estimated using FFT transform and found to be 0.30 and 0.26 nm, respectively (**Fig. S3**). Further, the (002) crystallite facet of exfoliated MoS_2 is ensured from the predominant peak exhibit at 2θ=14.4° from XRD spectra and no other crystallite orientations were noticed compared with bulk MoS_2 (**See supporting information S4.a**). The Figs. 1(c) and 1(d) shows the HRTEM images of CdS QDs and 2D-MoS_2 coated TiO_2 at two different locations. It clearly infers that TiO_2 exhibited anatase phase with (101) and (004) crystallite orientations and was confirmed through lattice space values of 0.35 and 0.23 nm, respectively. The crystallite structures of TiO_2 and TiO_2/CdS QDs composite electrodes were further examined with XRD (**See supporting information S4.b**). Among two crystallite phases (2H and 1T) of MoS_2 observed from Fig.1b, only 1T MoS_2 layer was noticed from TiO_2/CdS QDs interface (Fig.1c and 1d). Lin *et al* explored the phase transformation of 2H to 1T MoS_2 by gliding atomic planes during high temperature treatment, however to confirm the same in the present work more investigation is needed. Recent reports corroborate that 1T MoS_2 phase has best performance on electrocatalytic hydrogen production with substantial stability in water medium compare to 2H MoS_2.[8c, 12] Therefore, from Figs. 1(c) and 1(d), it is expected that 1T MoS_2 layer coated TiO_2/CdS QDs interfaces may perform efficient photoelectrocatalytic hydrogen generation. The elemental mapping at TiO_2/CdS/MoS_2 was recorded (Fig. 1(e)), which confirms the presence of Ti, O, Cd, Mo and S elements with uniform distribution.

The optical absorbance of pristine TiO_2, TiO_2/CdS and TiO_2/CdS/MoS_2 electrodes were evaluated from Kulbelka-Munk relation $(F(R)^{1/2} = [(1-R^2)/2R]^{1/2}$ using optical diffused reflectance spectra (Fig. 2a). The optical absorbance edge of TiO_2 at 380 nm is extended to ~495nm upon CdS QDs deposition (4 SILAR cycles). Owing to the high absorbance, CdS QDs enhanced the optical density of TiO_2 in this region. For 2 SILAR coated CdS cycles, the absorbance edge is blue shifted to ~450 nm due to the less deposition cycles of CdS. A significant band edge of MoS_2 (between 600 to 700 nm) was not observed in Fig. 2a.[13] This may attribute the less quantity of MoS_2 loading on TiO_2/CdS QDs or the metallic nature of 1T MoS_2 does not exhibit band gap alike exfoliated MoS_2 solution (**See supporting information S5**). It is noteworthy to discuss that the electrode geometry could influence the optical absorbance of back side electrode which depends with the light transmittance allowed by front side electrode **(See supporting information S6)**. In order to decipher the generic mechanism of visible light driven photocatalytic hydrogen fuel generation from TiO_2/CdS/ZnS/MoS_2 (*TCZM*) interfaces, we explored the photoelectrochemical property of this structure under dark and light conditions. Here, we used two electrode based PEC configuration (TiO_2/CdS(4 cycles)/ZnS as photoanode and TiO_2/CdS (2 cycles)/MoS_2 as counter electrode (CE) (**See Supporting Information S1(d)**). The aqueous electrolyte of 0.25 M Na_2S with 0.35 M Na_2SO_3 sacrificial hole scavenger was used

for PEC experiments. The electrodes were illuminated with artificial solar light (100 $mWcm^{-2}$) from solar simulator with 400 nm UV cut filter.

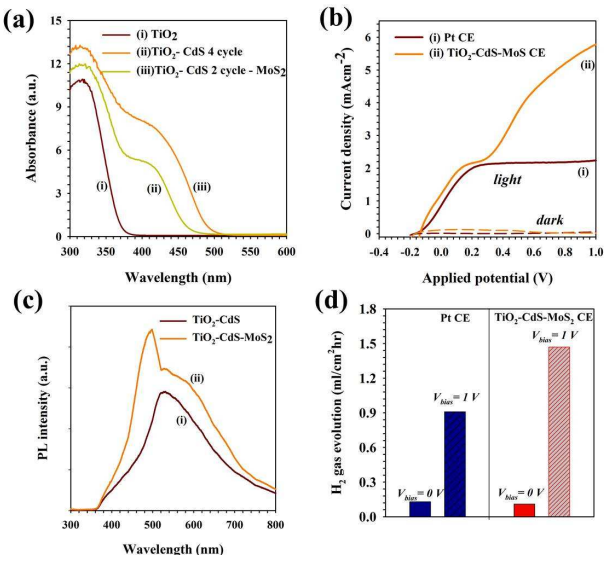

Figure 2. (a) Optical absorbance (Kulbelka-Munk) of pristine, CdS, and CdS/MoS_2 coated TiO_2; (b) J-V curves of PEC cells consist with TiO_2/CdS/ZnS photoanode with different counter electrodes; (c) Photoluminescence spectra of TiO_2/CdS in the presence and absence of MoS_2; (d) hydrogen gas evolution from PEC cells using TiO_2-CdS-ZnS photoanode with different counter electrodes (measured for 1 hour under visible light irradiation with UV cut-off filter).

The resultant PEC performance of *TCZM* CE is compared with *Pt* CE in Fig. 2(b). At zero potential, the *TCZM* showed ~0.8 $mAcm^{-2}$ and is almost comparable to the performance of similar photoanode configuration with Pt as CE. The solar to hydrogen (STH) efficiency of these electrodes was estimated using the relation:[5b]

$$STH = \frac{j_{sc} E^{o} \eta_{F}}{P_{total}} \qquad (1)$$

where, j_{sc} is the short-circuit current, E^{o} represents the thermodynamic reaction potential (0.21 V) for oxidation of sacrificial agent (G =38,600 J/mol), η_F is the faradic efficiency of hydrogen generation in standard condition and P_{total} is the incident solar irradiation (Wm^{-2}). The STH efficiency of TiO_2/CdS/MoS_2 CE found to be 0.45% and is comparable to Pt CE based system (STH= 0.44%). Comparing the conversion efficiency of MoS_2 catalyst to other previous reports on photocatalytic (PC) hydrogen generation; $Zn_{0.8}Cd_{0.2}S$ showed the STH efficiency of 0.36% with reduced graphene oxide (RGO) catalyst.[14] This implies that 1T MoS_2 had performed as co-catalyst at TiO_2/CdS (2 cycles) for generating hydrogen through Z-scheme under unassisted bias condition. Further, by applying electric potential between the two terminals of TiO_2/CdS/ZnS and Pt, the resulting photocurrent was found to be enhanced up to 2.2 $mAcm^{-2}$ at 0.2 V vs RHE. It infers that the applied potential facilitate the charge separation process at TiO_2/CdS interfaces by extracting the electrons away from CdS conduction band to TiO_2, which subsequently reaches CE terminal. In the case of *TCZM* hetrointerface, the applied potential enhances the Z scheme process (Scheme 1b) and generates high photocurrent density of 5.7 $mAcm^{-2}$ at 1 V vs RHE, compare to Pt CE (2.2 $mAcm^{-2}$). It clearly evinces that the photocurrent generation at *TCZM* hetrointerface depends on charge separation process at TiO_2/CdS cathode interface and showed competitive photocurrent generation with Pt CE. The photoexcited electron at CdS CB can reduce the H^+ ions to hydrogen owing to their negative conduction band position. However, it leads the photocorrosion on CdS surface. This undesired reaction was overwhelmed by the MoS_2 co-catalyst layer, which protects the CdS layer from water reduction process through modifying CdS/electrolyte interfaces. The modification of electrochemical TiO_2/CdS QDs interfaces by MoS_2 coating were analyzed with Mott-Schottky plots (**See supporting information Fig. S7**). The flat band potential (V_{fb}) position of TiO_2/CdS interface was found to be slightly modified from 0.05±0.03 V vs RHE to 0.09±0.03 V vs RHE by MoS_2. More positive values of V_{fb} position by MoS_2 coating indicates that the large band bending at MoS_2/CdS interfaces (depletion layer) facilitates the photoelectrons flow from CB of CdS to electrolyte for catalytic reduction of H^+ ions on MoS_2 sites. Further, to examine the influence of MoS_2 coating on TiO_2/CdS interfaces the PL spectra was recorded (Fig. 2c). The emission band shoulder around 530 nm was noticed from TiO_2/CdS interface, which can be attributed to the band–band PL phenomenon of CdS surface. This PL emission mostly originates from the sulphur vacancies of CdS which act as recombination centres to the photoelectrons.[15] Under identical excitation power, the MoS_2 coated TiO_2/CdS interface showed higher PL emission. One of the plausible reasons for the enhanced PL emission is reduced surface states at the CdS grain boundaries by occupying MoS_2.[10b] This infers that the MoS_2 can effectively passivate the CdS surface.

The output gas product from PEC experiments were collected for one hour and examined through gas chromatogram (GC. The output product was found to be hydrogen gas from the TiO_2/CdS hetrointerface and the quantity varies (Fig.2d) with counter electrodes and applied potential condition (**See supporting information S8**). Under unassisted potential condition, the Pt CE showed almost similar quantity of hydrogen gas (0.13 $mlhr^{-1}cm^{-2}$) than *TCZM* hetrointerface (0.15 $mlhr^{-1}cm^{-2}$). In striking contrast under identical conditions, the *TCZM* hetrointerface exhibited 1.47 $mlhr^{-1}cm^{-2}$ of hydrogen gas at 1 V vs RHE applied potential, which is 150 % higher than the hydrogen generated using Pt as CE (0.97 $mlhr^{-1}cm^{-2}$). This is in line with *J-V* results discussed from Fig. 2b, which ensured applied potential dependent hydrogen generation at *TCZM* hetrointerface. Another significant observation is that the electrode based *TCZM* hetrointerface maximises the fuel generation even with less material consumption (MoS_2 coated CdS QDs) compare to the earlier reports on solid state suspended photocatalysis. These results have significant implications in designing the MoS_2 co-catalyst based visible light semiconductor electrode architectures for hydrogen fuel generation with the aid of external bias from renewable sources (solar cells or solar batteries). The synergetic composition of 1-T MoS_2 with previously reported CuS or CuO

based electrodes will be futuristic Pt-free cathodes to QDs-sensitized metal oxide photoanodes in search of effective photoelectrodes in qusai-artificial photosynthetic leaf.[7, 16]

Conclusions

In summary, the 1-T metallic type MoS_2 nano-sheets were successfully assembled on TiO_2-CdS electrode. Under visible light irradiation, TiO_2-CdS-MoS_2 electrode exhibit efficient co-catalytic performance on hydrogen generation in configuration with TiO_2-CdS-ZnS photoanode. This tandem electrode configuration (TCZM) showed higher hydrogen fuel generation of 1.47 $mlhr^{-1}cm^{-2}$ at 1 V vs RHE applied potential, which is 150 % higher than that of using Pt as CE. In addition, 1-T MoS_2 sheets passivation at the TiO_2-CdS interface beneficially reduced the charge recombination through uncovered CdS sites on TiO_2 to electrolyte. Improving the photoanode counterpart with high porous network based electron transport framework (fibers, inverse opal) in association with narrow band gap semiconductor as co-sensitizers is anticipated to enhance the hydrogen fuel generation. Different temperature processed 1-T MoS_2 is also futuristic to promote hydrogen generation through fine-tuning their catalytic activity through modifying their edges.

Acknowledgements

One of the corresponding authors P.S appreciate the JSPS for provide the post-doctoral fellowship. R.R. thanks National Institute for Materials Science (NIMS), Japan and Anna University, India for the NIMS internship award.

Notes and references

[a] *Centre for Nanoscience and Technology,Anna University, Chennai, India 600 025; E-mail: rjvel@annauniv.edu*
[b] *Photocatalysis International Research Center(PIRC), Research Institute for Science & Technology, Tokyo University of Science, 2641 Yamazaki, Noda, Chiba 278-8510, Japan,; E-mail: vedichi@gmail.com*
[c] *International Center for Materials Nanoarchitectonics (WPI-MANA), National Institute for Materials Science (NIMS), 1-1 Namiki, Tsukuba, Ibaraki 305-0044, Japan.*

† Electronic Supplementary Information (ESI) available: [Experimental, Charecterization, XRD, SEM, TEM, PL,Chronoamperometry, OCVD]. See DOI: 10.1039/b000000x/

1 A. Fujishima and K. Honda, *Nature*, 1972, **238**, 37.
2 M. Gratzel, *Nature*, 2001, **414**, 338.
3 A. J. Cowan, J. Tang, W. Leng, J. R. Durrant and D. R. Klug, *The Journal of Physical Chemistry C*, 2010, **114**, 4208.
4(a) J. Hensel, G. Wang, Y. Li and J. Z. Zhang, *Nano Letters*, 2010, **10**, 478; (b) P. Rodenas, T. Song, P. Sudhagar, G. Marzari, H. Han, L. Badia-Bou, S. Gimenez, F. Fabregat-Santiago, I. Mora-Sero, J. Bisquert, U. Paik and Y. S. Kang, *Advanced Energy Materials*, 2013, **3**, 176; (c) Y. Jinnouchi, T. Hattori, Y. Sumida, M. Fujishima and H. Tada, *ChemPhysChem*, 2010, **11**, 3592; (d) P. Sudhagar, E. Juárez-Pérez, Y. Kang and I. Mora-Seró, in *Low-cost Nanomaterials*, eds. Z. Lin and J. Wang, Springer London, 2014, pp. 89-136.
5(a) R. Trevisan, P. Rodenas, V. Gonzalez-Pedro, C. Sima, R. S. Sanchez, E. M. Barea, I. Mora-Sero, F. Fabregat-Santiago and S. Gimenez, *The Journal of Physical Chemistry Letters*, 2012, **4**, 141; (b) V. González-Pedro, I. Zarazua, E. M. Barea, F. Fabregat-Santiago, E. de la Rosa, I. Mora-Seró and S. Giménez, *The Journal of Physical Chemistry C*, 2013, **118**, 891; (c) K. Kim, M.-J. Kim, S.-I. Kim and J.-H. Jang, *Sci. Rep.*, 2013, **3**.
6 K. Zhang and L. Guo, *Catalysis Science & Technology*, 2013, **3**, 1672.
7 M. Antoniadou, S. Sfaelou and P. Lianos, *Chemical Engineering Journal*, 2014, **254**, 245.
8(a) S. Das, M. Kim, J.-w. Lee and W. Choi, *Critical Reviews in Solid State and Materials Sciences*, 2014, **39**, 231; (b) K. F. Mak, C. Lee, J. Hone, J. Shan and T. F. Heinz, *Physical Review Letters*, 2010, **105**, 136805; (c) U. Maitra, U. Gupta, M. De, R. Datta, A. Govindaraj and C. N. R. Rao, *Angewandte Chemie International Edition*, 2013, **52**, 13057.
9(a) T. F. Jaramillo, K. P. Jørgensen, J. Bonde, J. H. Nielsen, S. Horch and I. Chorkendorff, *Science*, 2007, **317**, 100; (b) Y. Li, Y.-L. Li, C. M. Araujo, W. Luo and R. Ahuja, *Catalysis Science & Technology*, 2013, **3**, 2214; (c) D. Voiry, M. Salehi, R. Silva, T. Fujita, M. Chen, T. Asefa, V. B. Shenoy, G. Eda and M. Chhowalla, *Nano Letters*, 2013, **13**, 6222; (d) D. Merki and X. Hu, *Energy & Environmental Science*, 2011, **4**, 3878.
10(a) T. Jia, A. Kolpin, C. Ma, R. C.-T. Chan, W.-M. Kwok and S. C. E. Tsang, *Chemical Communications*, 2014, **50**, 1185; (b) Y. Min, G. He, Q. Xu and Y. Chen, *Journal of Materials Chemistry A*, 2014, **2**, 2578; (c) X. Zong, H. Yan, G. Wu, G. Ma, F. Wen, L. Wang and C. Li, *Journal of the American Chemical Society*, 2008, **130**, 7176; (d) X. Zong, G. Wu, H. Yan, G. Ma, J. Shi, F. Wen, L. Wang and C. Li, *The Journal of Physical Chemistry C*, 2010, **114**, 1963.
11 G. Eda, T. Fujita, H. Yamaguchi, D. Voiry, M. Chen and M. Chhowalla, *ACS Nano*, 2012, **6**, 7311.
12 M. A. Lukowski, A. S. Daniel, F. Meng, A. Forticaux, L. Li and S. Jin, *Journal of the American Chemical Society*, 2013, **135**, 10274.
13(a) G. Eda, H. Yamaguchi, D. Voiry, T. Fujita, M. Chen and M. Chhowalla, *Nano Letters*, 2011, **11**, 5111; (b) A. P. S. Gaur, S. Sahoo, M. Ahmadi, M. J. F. Guinel, S. K. Gupta, R. Pandey, S. K. Dey and R. S. Katiyar, *The Journal of Physical Chemistry C*, 2013, **117**, 26262.
14 J. Zhang, J. Yu, M. Jaroniec and J. R. Gong, *Nano Letters*, 2012, **12**, 4584.
15(a) G. Q. Xu, B. Liu, S. J. Xu, C. H. Chew, S. J. Chua and L. M. Gana, *Journal of Physics and Chemistry of Solids*, 2000, **61**, 829; (b) P. V. Kamat, N. M. Dimitrijevic and R. W. Fessenden, *The Journal of Physical Chemistry*, 1987, **91**, 396.
16(a) C. G. Morales-Guio, S. D. Tilley, H. Vrubel, M. Gratzel and X. Hu, *Nat Commun*, 2014, **5**; (b) A. Devadoss, P. Sudhagar, C. Ravidhas, R. Hishinuma, C. Terashima, K. Nakata, T. Kondo, I. Shitanda, M. Yuasa and A. Fujishima, *Physical Chemistry Chemical Physics*, 2014.